Efficient Charge Transport Enables High Efficiency in Dilute Donor Organic Solar Cells

Non Peer-reviewed author version

Yao, NN; Wang, JQ; Chen , Z; Bian, QZ; XIA, Yuxin; Zhang , R; Zhang, JQ; Qin, LQ; Zhu, HM; Zhang , Y & Zhang , FL (2021) Efficient Charge Transport Enables High Efficiency in Dilute Donor Organic Solar Cells. In: The journal of physical chemistry letters, 12 (20) , p. 5039 -5044.

DOI: 10.1021/acs.jpclett.1c01219
Handle: http://hdl.handle.net/1942/35841

Efficient charge transport and high efficiency in dilute donor organic solar cells

Nannan Yao[a], Jianqiu Wang[b], Zeng Chen[c], Qingzhen Bian[a], Yuxin Xia[d], Rui Zhang[a], Jianqi Zhang, Haiming Zhu[c,*], Yuan Zhang[b,*], Fengling Zhang[a,*]

[a] Department of Physics, Chemistry and Biology (IFM), Linköping University, Linköping, 58183, Sweden

[b] School of Chemistry, Beijing Advanced Innovation Center for Biomedical Engineering, Beihang University, Beijing, 100191, P. R. China

[c] State Key Laboratory of Modern Optical Instrumentation, Center for Chemistry of High-Performance & Novel Materials, Department of Chemistry, Zhejiang University, Hangzhou, 310027, P. R. China

[d] Institute for Materials Research (IMO-IMOMEC), Hasselt University, Diepenbeek, 3590, Belgium

Corresponding Authors

Haiming Zhu : E-mail: hmzhu@zju.edu.cn

Yuan Zhang : E-mail: yuanzhang@buaa.edu.cn

Fengling Zhang : E-mail: fengling.zhang@liu.se

ABSTRACT: Donor/acceptor (D/A) weight ratios are crucial for charge transport and photovoltaic performance of organic solar cells (OSCs). Here, we systematically investigate the photovoltaic behaviors of PM6:Y6 solar cells with different PM6 contents. It is found that the photovoltaic performance is tolerant to PM6 concentrations ranging from 10 wt%-60 wt%. Especially for the dilute donor-solar cells with only 10 wt% PM6, an impressive efficiency over 10% with high short circuit current density (J_{sc}) of 18.5 mA cm^{-2} and fill factor (FF) of 0.66 has been achieved. Efficient charge generation, electron/hole transport with slow charge recombination, and almost field-insensitive extraction can be achieved in 10 wt% donor solar cells. This raises the question about the origin of efficient hole transport in such dilute donor structure. By investigating on the hole mobility of PM6 diluted in Y6 and insulators, we find that effective hole transport pathway is mainly through PM6 phase in PM6:Y6 blends despite with low donor contents. The results indicate that a low fraction of polymer donors combines

with near-infrared non-fullerene acceptors could achieve high photovoltaic performance, that might be an candidate for semitransparent windows.

Keywords: efficient hole transport, low donor contents, non-fullerene acceptors, organic solar cells

1. Introduction

Organic solar cells (OSCs) based on non-fullerene acceptors (NFAs) have achieved rapid development in recent years due to the tunable energy levels and absorption spectra of NFAs [1–6]. The power conversion efficiency (PCE) of single-junction OSCs has reached over 17%18%？ [7–9]. The efficiency of OSCs is determined by the short circuit current density (J_{sc}), open-circuit voltage (V_{oc}) and fill factor (FF). In NFA-OSCs, efficient charge separation and low voltage losses can be achieved simultaneously, yielding high J_{sc} and V_{oc} [10–12]. The third important parameter FF is strongly affected by the competition between charge transport and recombination especially in low internal fields region (near V_{oc}). It has been demonstrated that efficient charge transport and suppressed recombination losses are largely related to balanced electron and hole mobility in OSCs [13,14]. Generally, a continuous interpenetrating network of donor and acceptor is considered to be significant for the electron and hole transport [15]. Therefore, the donor/acceptor blend composition is very important for the charge transport and device performance. Typically, in dilute donor heterojunctions where the average distance between individual donor domain enlarges, that may reduce hopping rate of hole. The unbalanced charge transport can induce space-charge effect, causing more recombination loss and poor performance [16]. Interestingly, some previous studies have reported that fullerene based OSCs with very low donor contents could maintain efficient hole transport [17,18]. It was proposed that hole tunneling could occur between isolated donors [19,20], another possible channel is that fullerene acceptors such as PCBM could act as an ambipolar conductor for both electrons and holes in dilute donor solar cells [17,21,22].

Compared to the clarification on the exclusive role of fullerene acceptors in dilute donor solar cells, charge generation, transport and recombination in dilute donor devices with NFAs are rarely investigated. Recently, NFA Y6 with A-D-A'-D-A configuration has received a great attraction. In the optimized solar cells based on PM6:Y6 (1:1.2, w/w), a high J_{sc} exceeding 25 mA cm^{-2} with a low voltage loss (~0.48 eV) can be achieved simultaneously [6,23]. A very recent report with single crystal analysis and molecular simulation has highlighted the unique packing in Y6 films can lead to strong electronic coupling between adjacent Y6 molecules and efficient 3-dimensional ambipolar transport networks [24]. These interesting phenomena raise an important question about hole transport mechanisms in bulk heterojunctions (BHJs) with this emerging family of NFAs, which could contribute to the high device performance. Dilute donor solar cells are interesting models to understand the role of acceptors on charge generation, transport and extraction. Therefore, it will be informative to investigate the correlation between photovoltaic performance and donor/acceptor blend composition in NFA-OSCs.

In this work, we studied the photovoltaic behaviors of PM6:Y6 solar cells with various PM6 contents. OSCs with 10 wt% PM6 yield a high PCE of 10.3 % with J_{sc} of 18.5 mA cm^{-2} and FF of 0.66. The results of femtosecond transient absorption (TA) spectroscopy indicate long exciton diffusion process and efficient exciton dissociation in dilute donor blend films. In contrast, the PM6:Y6 solar cells with high donor weight ratio (90 wt%) show faster charge recombination. Moreover, slow charge recombination in dilute D solar cells was proved by light intensity-dependent measurement and transient photovoltage (TPV). Almost field-independent charge transport and extraction in the dilute donor devices were observed by transient photocurrent (TPC) and bias-dependent EQE, whereas the carrier sweepout in the 90 wt% PM6 devices is associated with a much stronger dependence on the electrical field, indicating large amounts of recombination loss. Importantly, it is found that PM6:Y6 blend even with 10 wt% PM6 exhibits efficient hole transport and balanced charge transport. By comparation the hole

mobility of PM6 diluted at 10 wt% in Y6 and insulating polymers, we conclude that 10 wt% PM6 in PM6:Y6 blends can still retain efficient hole transport pathway through the active layer, that is also confirmed by measuring grazing-incidence wide-angle X-ray scattering (GIWAXS).

2. Results and Discussion

2.1. Photovoltaic performance of PM6:Y6 solar cells with various PM6 contents

PM6:Y6 solar cells with various PM6 contents were fabricated with a standard structure of ITO/PEDOT:PSS/active layer/PDINO/Al. Fig. S1 shows *J-V* curves of PM6:Y6 solar cells with different PM6 contents under AM 1.5 G solar irradiation (100 mW cm^{-2}). The photovoltaic parameters extracted from *J-V* curves are summarized in Fig. 1 and Table S1. As shown, the photovoltaic performance of PM6:Y6 solar cells exhibit a high tolerance to donor contents ranging from 10 wt%-60 wt%. The pristine Y6 devices exhibit negligible J_{sc} and efficiency due to the poor exciton separation. Upon addition of 5 wt% PM6, the J_{sc} dramatically increases from 0.25 mA cm^{-2} to 11.35 mA cm^{-2} and FF increases to 0.52. Solar cells with 10 wt% PM6 yield an efficiency over 10% with high J_{sc} of 18.5 mA cm^{-2} and FF of 0.66. It is worth noting that the dilute donor devices show much better photovoltaic performance than the devices with high donor contents, especially for J_{sc} and FF, that are largely determined by charge generation dynamics and the competition between charge transport and recombination. To understand the origin of high performance of OSCs with such low donor contents, charge generation, transport and recombination were investigated in following sections.

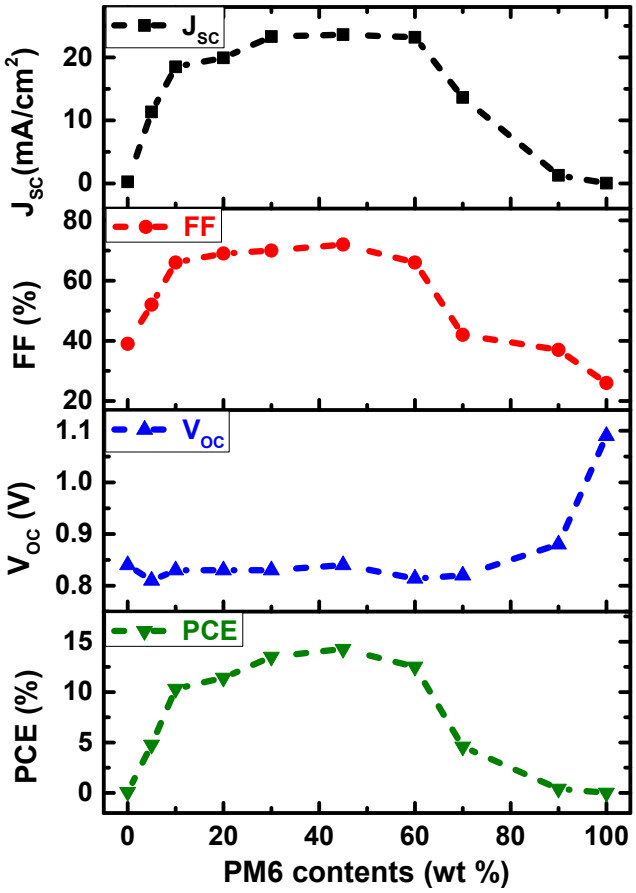

Fig. 1. Correlation between photovoltaic performance of PM6:Y6 solar cells and PM6 contents (under 100 mW cm^{-2} solar illumination). The dashed lines are guides to the eye.

2.2. Charge generation

To investigate charge transfer between PM6 and Y6, steady-state photoluminescence (PL) spectroscopy was employed (Fig. S2). Compared to the PL of pure Y6 films, the PL intensity of PM6:Y6 blends show a decrease trend with the amount of donor content increased from 5 wt% to 45 wt%. The PL intensity of BHJ with 10 wt% PM6 was quenched by 85%, suggesting efficient interfacial charge transfer. Hole transfer dynamics from Y6 to PM6 was studied with femtosecond TA spectroscopy. In Fig. S3, a 750 nm pump laser was used to selectively excited Y6. The rising kinetics of PM6 ground state bleach in the blend at ~605 nm reflects the hole

transfer from Y6 to PM6, since photoexcited Y6 shows no absorption signal there. Hole transfer process consists of an ultrafast hole transfer process and a diffusion mediated process. Hole transfer kinetics (Table S2) were fitted by a biexponential function

$$I = A_1 \exp(-\frac{t}{\tau_1}) + A_2 \exp(-\frac{t}{\tau_2})$$

with two lifetimes of τ_1 and τ_2 and prefactors of A_1 and A_2 [25,26]. Ultrafast charge transfer process indicated by τ_1 should be attributed to quantum coherence, which plays a role in the formation of charge carriers [27] and was experimentally observed in the solar cells [28]. In Fig. 2a, all blend films with different PM6 wt% show ultrafast charge transfer process in the timescale of 100 fs-250 fs. The following exciton diffusion process characterized by A_2 and τ_2 becomes more dominant with the decreasing of PM6 contents. In Fig. 2b, the exciton diffusion lifetimes τ_2 in dilute donor blends are much longer than that in blends with 90 wt% PM6, which is strongly related to the domain sizes in BHJs [26]. The fitting results in Table S2 indicate that dilute donor blends exhibit longer hole transfer lifetime, suggesting efficient hole transfer.

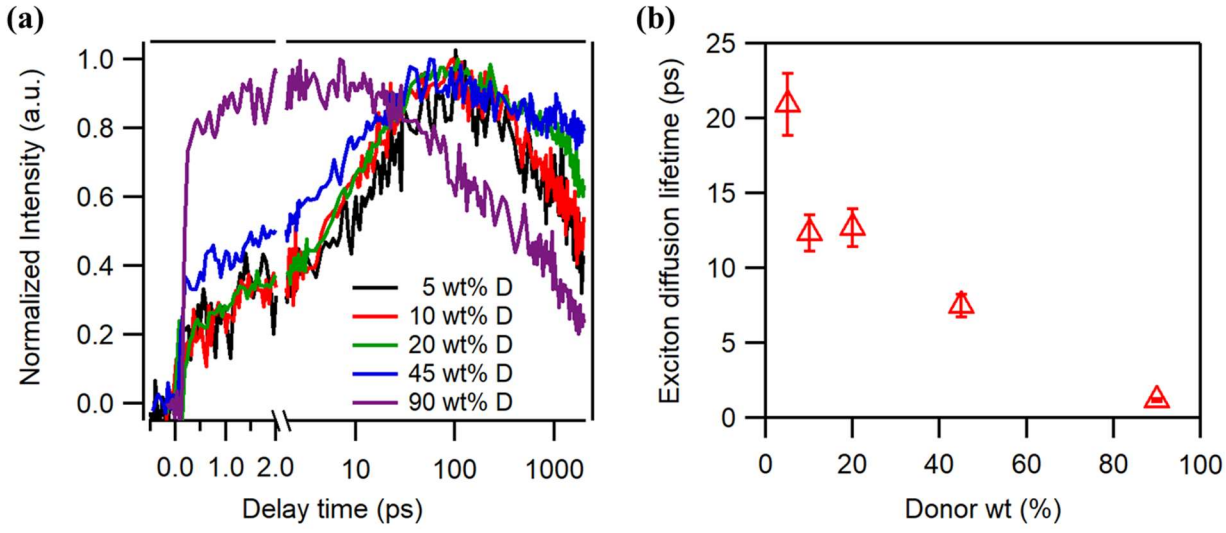

Fig. 2. (a) Normalized TA kinetics of hole transfer in PM6:Y6 blend films with various PM6 contents (pump at 750 nm, probe at 605 nm); (b) Exciton diffusion lifetime as a function of PM6 contents (wt %).

As mentioned above, the exciton diffusion process is related to the domain sizes, surface topographies . Blend films were measured by atomic force microscopy (AFM). As illustrated in Fig. S4, the domain size in these blend films decreases with the increasing donor contents. Large domain size in BHJ films with 10 wt% PM6 means that excitons will be created away from the interface and thus spend longer time to diffuse to the interfaces. It has been demonstrated that Y6 shows long exciton diffusion length of 35 nm [29], therefore, even in dilute donor blends with large domain size, charge transfer can still retain efficient. However, the blend film with 90 wt% PM6 shows much smaller domain size, as a result, excitons have more probability of diffusing to the interface, leading to fast interfacial charge recombination. Moreover, the decay signals in Fig. 2a should be attributed to charge recombination loss. PM6:Y6 blend films with low donor contents behave slower decay than 90 wt% PM6-based BHJs, suggesting slower charge recombination in dilute donor blends.

2.3. Charge transport and recombination

To investigate the charge transport, charge carrier mobilities were determined from space charge limited current (SCLC) in single-carrier devices, as shown in Fig. S5 and Fig.3. Interestingly, the hole mobilities have little correlation with the PM6 contents, the devices even with 10 wt% PM6 can still exhibit high electron mobility of 2.7×10^{-4} cm^2 V^{-1} s^{-1} and hole mobility of 6.8×10^{-5} cm^2 V^{-1} s^{-1} (Table S2), indicating efficient charge transport in such dilute donor structure. However, the electron mobilities show an obvious decrease when PM6 contents is over 60 wt%, the unbalanced charge transport results in a decreased device performance (Fig.1). It is worth noting that pristine Y6 devices show both high electron mobility (6.5×10^{-4} cm^2 V^{-1} s^{-1}) and hole mobility (1.8×10^{-4} cm^2 V^{-1} s^{-1}), indicating Y6's ambipolar property.

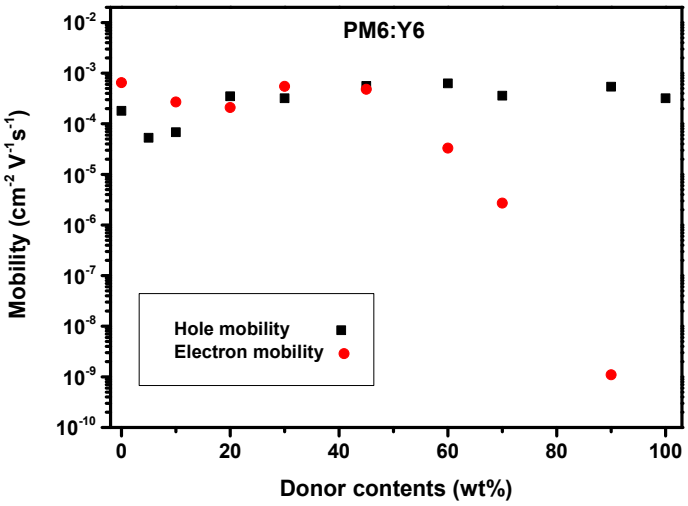

Fig.3 Electron and hole mobilities in PM6:Y6 OSCs with various donor contents extracted from SCLC in single-carrier devices.

The charge transport blend films significantly influences charge recombination and extraction in solar cells. To study the charge recombination in device operational conditions, we examined irradiation power (I)-dependent V_{oc} and J_{sc} in three representative PM6:Y6 BHJ devices (10 wt%, 45 wt% and 90 wt% PM6). Typically, the relationship between J_{sc} and I can be described by power law as $J_{sc} \propto I^{\alpha}$, where the deviation from α=1 is due to recombination loss. As shown in Fig. 4a, the solar cells with 10 wt% and 45 wt% PM6 show similar α value of 0.94 and 0.95. The high α approaching to unity indicates smaller bimolecular recombination loss, that should be due to balanced electron/hole transport in in these two cases. It has been demonstrated that the J_{sc} of non-space-charge limited devices is linearly dependent on I, while space-charge limited photocurrents in OSCs caused by unbalanced mobility of electrons and holes have a irradiation dependence following ~$I^{0.75}$ [16,30]. The relatively low α=0.76 in the device based on 90 wt% PM6 implies stronger recombination. Therefore, we propose that there is the emergence of strong space-charges effect in 90 wt% donor devices mainly caused by extremely unbalanced charge transport.

Light intensity-dependence of V_{oc} can be described by the Shockley equation,

$$V_{oc} = n\frac{kT}{q}\ln(\frac{J_{sc}}{J_s} + 1)$$

where J_s is the reverse saturation current density, q is the elementary charge, k is Boltzmann's constant, T is temperature and n is an ideality factor [31]. The ideality factor n=1 indicates bimolecular recombination dominated and n=2 implies trap-assisted recombination.[31,32] Typically, these types of recombination co-exist in OSCs and n is usually between 1 and 2. In Fig. 4b, the slopes of PM6:Y6 devices with 10 wt% and 45 wt% donor are around 1.3, indicating that the recombination is primarily via the bimolecular pathways with a minor role of trap-assisted recombination. The n-value of the dilute A device (90 wt% PM6) is very close to unity, which suggests that in the donor-dominant matrix, photogenerated carriers are purely lost via bimolecular recombination.

Moreover, TPV measurements were performed on PM6:Y6 solar cells as shown in Fig. 4c, where the photovoltage decay is due to the recombination loss and longer decay time indicates slower charge recombination. The solar cells with 10 wt% and 45 wt% PM6 exhibit slower recombination with longer decay time of 49.1 μs and 75.5 μs, respectively, however, the device with 90 wt% PM6 shows much faster charge recombination with a shorter decay time of 31.6 μs, which agrees with the above results.

In the case of extremely unbalanced D/A ratios, discontinuous interpenetrating network of donor and acceptor might be an important issue for charge transport. Also, a reduced contact area of anode/D or cathode/A could lead to a low charge extraction efficiency. Here we investigated charge extraction processes by using bias-dependent TPC measurements (Fig. S6), charge extraction time versus bias were obtained from TPC with a mono-exponential decay model. In Fig. 4d, the most notable difference is that compared to the device with 90 wt% PM6, the solar cells with 10 wt% and 45 wt% PM6 contents show faster and nearly field- independent charge transport and extraction, especially near the low internal field region. These results are

in consistent with the bias-EQE results as shown in Fig. S7. This feature can arise from the suppressed recombination loss at low internal fields, so that photo-generated carriers can be collected more efficiently, yielding high J_{sc} (18.5 mA cm^{-2}) and FF (0.66) in OSCs with10 wt% PM6.

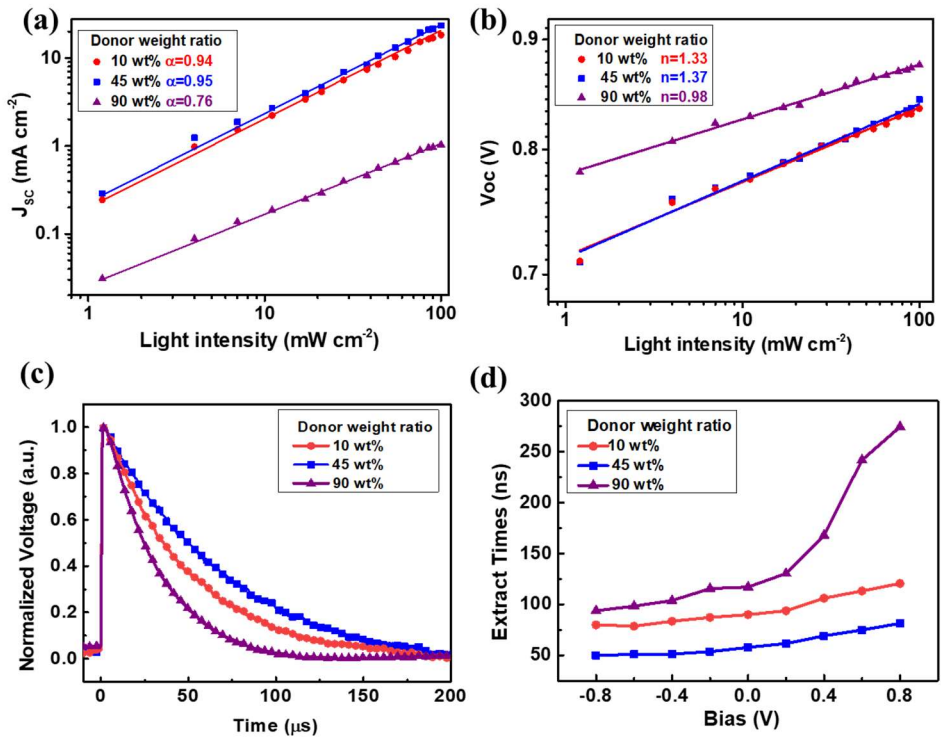

Fig. 4. Light intensity-dependent (a) J_{sc} and (b) V_{oc} characteristics of PM6:Y6 solar cells with various PM6 weight ratios; (c) TPV under open-circuit conditions; (d) Charge extraction time (τ_{ext}) as function of external bias in the studied solar cells determined from TPC measurements.

Above results have been demonstrated that the dilute donor devise with 10 wt% PM6 show high and balanced charge transport. As for the origin of efficient hole transport in dilute donor devices, we assume that the hole transport pathways in dilute donor solar cells can be depicted as Fig.6 shown, hole tunneling can occur between isolated donors (i) and holes can transport directly in donor phase (ii). In addition, the distinctive hole transport in Y6 may facilitate the hole transport in the BHJ blend, therefore, another possible pathway is that Y6 act as an

ambipolar conductor in the dilute donor blends to transport both electrons and holes to the cathode and anode (iii), respectively.

To clarity the hole transport mechanism in PM6:Y6 solar cells with 10 wt% PM6, we compared the hole mobilities of PM6 diluted by Y6 and polystyrene (PS), with 10 wt% PM6. Here, PS is an insulator with very low hole mobility in the order of 10^{-8} cm^2 V^{-1} s^{-1}, so that the dominant hole transport pathways in dilute donor devices can be investigated. As the results shown in Fig.S8 and Table 1, the hole mobilities of both PM6:Y6 and PM6:PS with 1:9 weight ratios are in the same order of magnitude, which are comparable to the hole mobility of pristine PM6, indicating the holes transport in PM6 phase is the dominant mechanism in PM6:Y6 blends with 10 wt% donor. To further confirm this conclusion, we also check the hole mobility of PM6 diluted by another insulator polymethyl methacrylate (PMMA). The hole-only devices based on PM6:PMMA BHJs with 10 wt % PM6 were fabricated and the result was also shown in Table 1, PM6:Y6 and PM6:PMMA blends with 10 wt % PM6 also show comparable hole mobilities. Therefore, we conclude that PM6:Y6 blends even with 10 wt% PM6 can still maintain efficient hole transport and a small amount of PM6 can form the continuous hole transport pathway.

Table 1 Hole mobilities of pristine PM6, PS, PMMA and PM6:Y6, PM6:PS, PM6:PMMA BHJs with 10 wt% PM6

	PM6	**PS**	**PMMA**	**PM6:Y6**	**PM6:PS**	**PM6:PMMA**
μ_h **[cm^2 V^{-1} s^{-1}]**	3.2×10^{-4}	9.2×10^{-8}	1.6×10^{-8}	6.8×10^{-5}	1.2×10^{-4}	3.7×10^{-5}

The PM6 continuous pathway in dilute devices also can be confirmed by GIWAXS (Fig. 5). In 1:1.2 PM6:Y6 blend system (45 wt% PM6), both (100) diffraction peak in in-plane direction (0.29 nm^{-1}) and (010) diffraction peak in out-of-plane direction (1.74 nm^{-1}) are obviously

observed, as well as a strong (111) diffraction in in-plane for Y6, which means relatively ordered transport structure for free charges. In diluted acceptor blend (90 wt% PM6), the donor component exists a strong signal along with in-plane ((100) at 0.29nm^{-1}) direction and out-of-plane ((010) 1.74 nm^{-1}), meaning a high crystallinity for the PM6 molecules. Moreover, in diluted donor blend (10 wt% PM6), in addition to the diffraction signals for Y6 molecules ((111) at 0.42 nm^{-1} in in-plane and (020) at 0.22 nm^{-1} in out-of-plane, we also observe the (100) diffraction peak at 0.33 nm^{-1} in in-plane for PM6, which mostly induced by the face-oriented Y6 molecules. This phenomenon reveals that although in dilute donor blend matrix, the donor exhibit ordered structure. Therefore, PM6 could support efficient hole transport pathway even at low donor contents, this can account for high hole mobility in dilute donor devices.

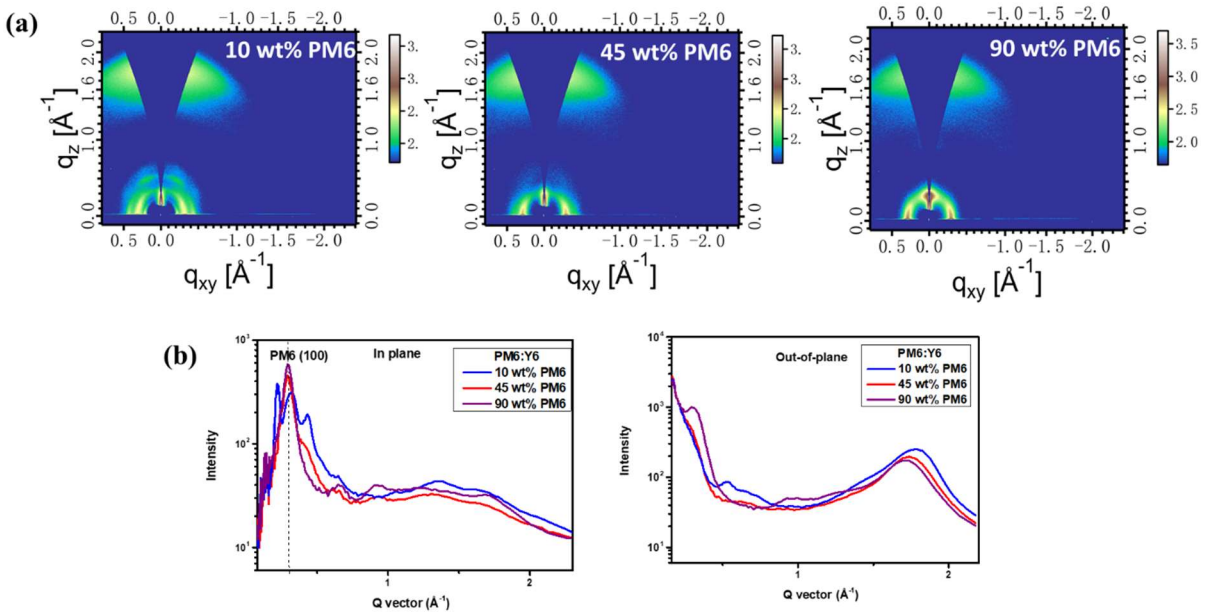

Fig. 5. (a) 2D GIWAXS patterns and (b) out-of-plane and in-plane of PM6:Y6 blend films with 10 wt%, 45 wt%, 90 wt% PM6.

Given the discussions above, we propose a transport model in dilute donor solar cells as illustrated in Fig. 6a, the photogenerated holes can hop from a specific site to its neighbors (i),

another channel is that hole can transport in donor phase that directly access the contacts (ii). Even though the pristine acceptor can support ambipolar transport, the hole transport pathway via acceptor phase (iii) has no obvious contribution to hole transport in this dilute donor structure.??? Reasons???energetic barrier for A-D.. A small amount of donor can support efficient hole transport pathway, enabling well-balanced charge transport with sufficiently high mobilities in the dilute donor devices. By contrast, in device with 90 wt% donor (Fig. 6b), unlike the long chain of polymer donor, small molecular acceptors are forming discontinuous pathways for electron transport. The generated electrons will be difficult to transport through isolated acceptor domains. The large difference in electron/hole mobilities give rise to formation of space-charge limited photocurrent and more recombination loss, limiting device performance. The results illustrate efficient hole transport via donor phase in dilute donor organic solar cells.

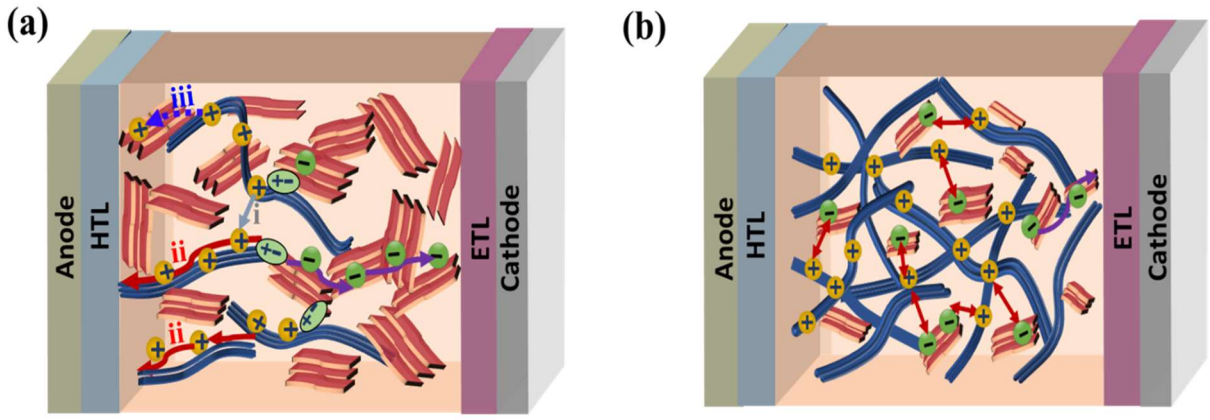

Fig. 6. Schematic diagram for charge transport pathways in (a) dilute donor solar cells: hole transport toward the anode side can either happen by tunneling between isolated donors (i, grey arrows); hole transport directly in donor phase touching the anode contacts (ii, red arrows). Electron transport via acceptors is indicated by purple arrows. (b) dilute acceptor solar cells: continuous donor networks support hole transport, while efficient electron transport can only happen in acceptor touching cathode contacts (purple arrows). Discontinuous pathways for electron transport lead to charge recombination loss as illustrated by red double arrows.

3. Conclusions

The photovoltaic behaviors of PM6:Y6 solar cells with varying PM6 contents were comparatively studied. A surprisingly high PCE exceeding 10% with high J_{sc} of 18.5 mA cm^{-2} and FF of 0.66 was achieved in the dilute donor devices with 10 wt% PM6. Intensive investigation on charge generation, transport and extraction was conducted to understand the strikingly different behaviors of above solar cells with varied stoichiometries. The results of TA, TPV, TPC and bias-dependent EQE reveal efficient hole transfer, charge transport with slow charge recombination and almost field-insensitive extraction in dilute donor devices. Importantly, electron and hole mobility measurements on single carrier devices prove that PM6:Y6 solar cells with 10 wt% PM6 show relatively balanced charge transport with high electron mobility and hole mobility. By comparation the hole mobility of 10 wt% PM6 blend with Y6, PS and PMMA, we demonstrate that the dominant holes transport in dilute PM6:Y6 blends is through PM6 interconnecting network with good order. Efficient photovaltic performance of dilute donor heterojunctions may help generate new application perspectives such as for near-infrared photodetectors or semitransparent photovoltaic devices.

4. Experimental Section

4.1. Materials

PM6, PBDBT, IT-4F, PFN-Br and PDINO were purchased from Solarmer, Inc (Beijing). Y6 was purchased from The Hong Kong University of Science and Technology (HKUST). All

materials were used as received without additional purification. PEDOT:PSS was purchased from Heraeus (CLEVIOSTM PVP Al 4083).

4.2. Device fabrication

OSCs were prepared with conventional structure of ITO/PEDOT:PSS/PM6:Y6/PDINO/Al. The ITO-coated glasses were cleaned by detergent and then treated by TL-1 with a mixture of water, ammonia, and hydrogen peroxide (volume ratio 5:1:1). PEDOT:PSS was spin-coated on ITO at 4000 rpm for 30 s, followed by annealing at 150 °C for 15 min. PM6:Y6 with different donor concentrations were dissolved in chloroform with a total concentration of 16-18 mg/mL. 0.5% CN (volume ratio) was used as additive in blend solution. The active layers were spin-coated on ITO/PEDOT:PSS and then were thermally annealed at 110 °C for 10 min in glovebox. After that PDINO (1.5 mg/mL in methanol) was spin-coated on the active layers at 3000 rpm. Finally, 100 nm of Al was thermally evaporated through shadow mask in a vacuum 1×10^{-6} mbar. The effective device area of devices is 0.047 cm^2. For electron-only devices, ZnO acted as electron transport layer was spin-coated on the ITO substrates and then were thermally annealed at 120 °C for 30 min. The active layers were spin-coated on ITO/ZnO, followed by annealing at 110 °C for 10 min. After spin coating PDINO, Al electrode was deposited to form the configuration of ITO/ZnO/Active layers/PDINO/Al. For hole-only devices (ITO/PEDOT:PSS/Active layer/MoO_3/Ag), MoO_3 and Ag were deposited by evaporation under a pressure ca. 1×10^{-6} mbar.

4.3. Characterization

The Current density-voltage (*J-V*) curves were characterized by a Keithley 2400 source meter with AM 1.5G solar simulator at an intensity of 100 mW/cm^2. The EQE spectra were recorded using a Newport Merlin lock-in amplifier. Single carrier devices were examined with a Keithley 2400 Source Meter in dark. To determine the mobility, we adopted the widely used space-charge limited current (SCLC) method with the relation

$$J = \frac{9}{8}\varepsilon_0\varepsilon_r\mu\frac{(V - V_{bi})^2}{d^3}$$

here ε_0, ε_r are the vacuum permittivity and dielectric constant of semiconductor, respectively, and d is the thickness of active layer. For electron-only solar cells based on pristine donors, there is not space-charge region, therefore, we can not get the μ_e of pristine donors.

PL spectra (excitation at 532 nm) were measured by using an Andor Solis SR393i-B spectrograph with a Newton EM-CCD Si array detector.

For femtosecond transient absorption spectroscopy, the fundamental output from Yb:KGW laser (1030 nm, 220 fs Gaussian fit, 100 kHz, Light Conversion Ltd) was separated to two light beam. One was introduced to NOPA (ORPHEUS-N, Light Conversion Ltd) to produce a certain wavelength for pump beam (here we use 750 nm, below 10 μJ/cm^2/pulse, 30 fs pulse duration), the other was focused onto a YAG plate to generate white light continuum as probe beam. The pump and probe overlapped on the sample at a small angle les s than 10°. The transmitted probe light from sample was collected by a linear CCD array.

TPC and TPV measurements were performed on a customized transient measurement systems (Physike Technology Co., Ltd) by using a pulsed semiconductor laser S3 (Coherent, Inc.).

TOC

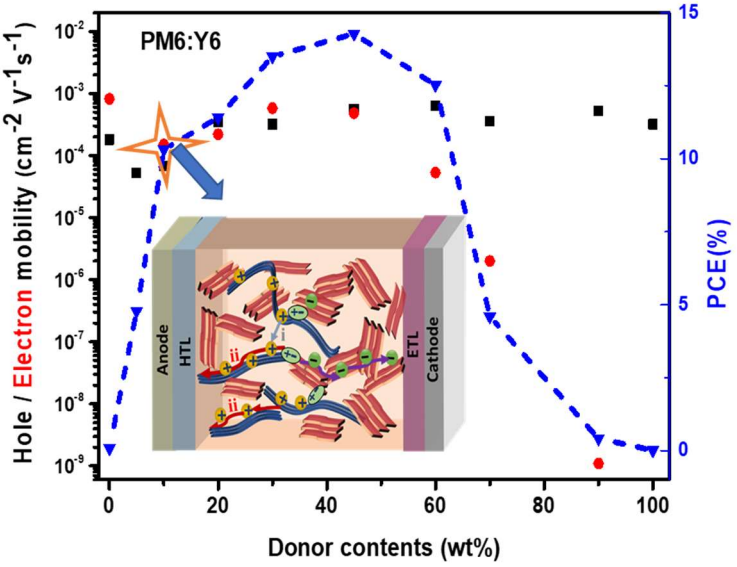

Acknowledgements

N. Y. and F. Z. acknowledge funding from the Knut and Alice Wallenberg foundation under contract 2016.0059, the Swedish Government Research Area in Materials Science on Functional Materials at Linköping University (Faculty Grant SFO-Mat-LiU No. 200900971) and China Scholarship Council (CSC) (No. 201708370115). Y. Z. thanks the financial support by the National Natural Science Foundation of China (No. 21875012, 21674006). H. Z. acknowledges the financial support by the National Key Research and Development Program of China (2017YFA0207700).

References

[1] Y. Lin, J. Wang, Z.G. Zhang, H. Bai, Y. Li, D. Zhu, X. Zhan, Adv. Mater. 27 (2015) 1170-1174.

[2] S. Li, L. Ye, W. Zhao, S. Zhang, S. Mukherjee, H. Ade, J. Hou, Adv. Mater. 28 (2016) 9423-9429.

[3] W. Zhao, S. Li, H. Yao, S. Zhang, Y. Zhang, B. Yang, J. Hou, J. Am. Chem. Soc. 139 (2017) 7148-7151.

[4] J. Hou, O. Inganas, R.H. Friend, F. Gao, Nat. Mater. 17 (2018) 119-128.

[5] J. Yuan, Y. Zhang, L. Zhou, C. Zhang, T.K. Lau, G. Zhang, X. Lu, H.L. Yip, S.K. So, S. Beaupré, M. Mainville, P.A. Johnson, M. Leclerc, H. Chen, H. Peng, Y. Li, Y. Zou, Adv. Mater. 31 (2019) 1807577.

[6] J. Yuan, Y. Zhang, L. Zhou, G. Zhang, H.L. Yip, T.K. Lau, X. Lu, C. Zhu, H. Peng, P.A. Johnson, M. Leclerc, Y. Cao, J. Ulanski, Y. Li, Y. Zou, Joule 3 (2019) 1140-1151.

[7] Y. Cui, H. Yao, L. Hong, T. Zhang, Y. Tang, B. Lin, K. Xian, B. Gao, C. An, P. Bi, W. Ma, J. Hou, Natl. Sci. Rev. 7 (2019) 1239-1246.

[8] C. Zhu, J. Yuan, F. Cai, L. Meng, H. Zhang, H. Chen, J. Li, B. Qiu, H. Peng, S. Chen, Y. Hu, C. Yang, F. Gao, Y. Zou, Y. Li, Energy Environ. Sci. 13 (2020) 2459-2466.

[9] Y. Lin, Y. Firdaus, F.H. Isikgor, M.I. Nugraha, E. Yengel, G.T. Harrison, R. Hallani, A. El-Labban, H. Faber, C. Ma, X. Zheng, A. Subbiah, C.T. Howells, O.M. Bakr, I. McCulloch, S.D. Wolf, L. Tsetseris, T.D. Anthopoulos, ACS Energy Lett. 5 (2020), 2935-2944.

[10] J. Liu, S. Chen, D. Qian, B. Gautam, G. Yang, J. Zhao, J. Bergqvist, F. Zhang, W. Ma, H. Ade, O. Inganäs, K. Gundogdu, F. Gao, H. Yan, Nat. Energy 1 (2016) 16089.

[11] Y. Li, D. Qian, L. Zhong, J.D. Lin, Z.Q. Jiang, Z.G. Zhang, Z. Zhang, Y. Li, L.S. Liao, F. Zhang, Nano Energy 27 (2016) 430-438.

[12] J. Yuan, T. Huang, P. Cheng, Y. Zou, H. Zhang, J.L. Yang, S.Y. Chang, Z. Zhang, W. Huang, R. Wang, D. Meng, F. Gao, Y. Yang, Nat. Commun. 10 (2019) 570.

[13] D. Bartesaghi, I.D.C. Pérez, J. Kniepert, S. Roland, M. Turbiez, D. Neher, L.J.A. Koster, Nat. Commun. 6 (2015) 7083.

[14] J. Wang, N. Yao, D. Zhang, Z. Zheng, H. Zhou, F. Zhang, Y. Zhang, ACS Appl. Mater. Interfaces 12 (2020) 38460-38469.

[15] J. Zhang, H.S. Tan, X. Guo, A. Facchetti, H. Yan, Nat. Energy 3 (2018) 720-731.

[16] V.D. Mihailetchi, J. Wildeman, P.W.M. Blom, Phys. Rev. Lett. 94 (2005) 126602.

[17] K.G. Jespersen, F. Zhang, A. Gadisa, V. Sundström, A. Yartsev, O. Inganäs, Org. Electron. 7 (2006) 235-242.

[18] T. Albes, L. Xu, J. Wang, J.W.P. Hsu, A. Gagliardi, J. Phys. Chem. C 122 (2018) 15140-15148.

[19] A. Melianas, V. Pranculis, D. Spoltore, J. Benduhn, O. Inganäs, V. Gulbinas, K. Vandewal, M. Kemerink, Adv. Energy Mater. 7 (2017) 1700888.

[20] D. Spoltore, A. Hofacker, J. Benduhn, S. Ullbrich, M. Nyman, O. Zeika, S. Schellhammer, Y. Fan, I. Ramirez, S. Barlow, M. Riede, S.R. Marder, F. Ortmann, K.Vandewal, J. Phys. Chem. Lett. 9 (2018) 5496-5501.

[21] S.M. Tuladhar, D. Poplavskyy, S.A. Choulis, J.R. Durrant, D.D.C. Bradley, J. Nelson, Adv. Funct. Mater. 15 (2005) 1171-1182.

[22] X. Guo, M. Zhang, J. Tan, S. Zhang, L. Huo, W. Hu, Y. Li, J. Hou, Adv. Mater. 24 (2012) 6536-6541.

[23] A. Karki, J. Vollbrecht, A.L. Dixon, N. Schopp, M. Schrock, G.N.M. Reddy, T. Nguyen, Adv. Mater. 31 (2019) 1903868.

[24] G. Zhang, X.K. Chen, J. Xiao, P.C.Y. Chow, M. Ren, G. Kupgan, X. Jiao, C.C.S. Chan, X. Du, R. Xia, Z. Chen, J. Yuan, Y. Zhang, S. Zhang, Y. Liu, Y. Zou, H. Yan, K.S. Wong, V. Coropceanu, N. Li, C.J. Brabec, J.L. Bredas, H.L. Yip, Y. Cao, Nat. Commun. 11

(2020) 3943.

[25] Y. Zhong, M.T. Trinh, R. Chen, G.E. Purdum, P.P. Khlyabich, M. Sezen, S. Oh, H. Zhu, B. Fowler, B. Zhang, W. Wang, C.Y. Nam, M.Y. Sfeir, C.T. Black, M.L. Steigerwald, Y.L. Loo, F. Ng, X.Y. Zhu, C. Nuckolls, Nat. Commun. 6 (2015) 8242.

[26] Z. Chen, X. Chen, B. Qiu, G. Zhou, Z. Jia, W. Tao, Y. Li, Y.M. Yang, H. Zhu, J. Phys. Chem. Lett. 11 (2020) 3226-3233.

[27] J.L. Brédas, E.H. Sargent, G.D. Scholes, Nat. Mater. 16 (2017) 35-44.

[28] Q. Bian, F. Ma, S. Chen, Q. Wei, X. Su, I.A. Buyanova, W.M. Chen, C.S. Ponseca, M. Linares, K.J. Karki, A. Yartsev, O. Inganäs, Nat. Commun. 11 (2020) 617.

[29] Firdaus, Y., Le Corre, V.M., Karuthedath, S. et al. Long-range exciton diffusion in molecular non-fullerene acceptors. Nat Commun 11, 5220 (2020).

[30] L.J.A. Koster, V.D. Mihailetchi, H. Xie, P.W.M. Blom, Appl. Phys. Lett. 87 (2005) 203502.

[31] L.J.A. Koster, V.D. Mihailetchi, R. Ramaker, P.W.M. Blom, Appl. Phys. Lett. 86 (2005) 123509.

[32] S.R. Cowan, A. Roy, A.J. Heeger, Phys. Rev. B 82 (2010) 245207.